University of Michigan
Department of Mechanical Engineering
Cavitation and Multiphase Flow Laboratory

Report No. UMICH 014456-45-I

# Influence of Cavitation Erosion on Corrosion Fatigue and Effects of Resistance to that Influence by the Surface Coatings

T. Okada , K. Awazu , H. Kawasaki

Tsunenori OKADA: University of Fukui, Faculty of Engineering, Mechanical Department, Bunkyo 3-9-1, Fukui. Professor.

Kaoru AWAZU: Industrial Research Institute, Ishikawa, Yoneizumi 4-133, Kanazawa. Engineer.

Hisamitsu KAWASAKI: Toyoda Koki Co., Ltd., Asahi 1-1, Kariya, Aichi Prefecture. Engineer

"Office of Naval Research Contract NO. N00014-78-C-0697

June, 1979

ABSTRACT

When fatigue tests are carried out under cavitation erosion in 3% salt water, the fracture of S35C test pieces occurs in the area of corrosion, as in the case of corrosion fatigue without cavitation erosion. However, the erosion fatigue strength decreases more than the corrosion fatigue strength by means of the formation of a macro-galvanic cell between the erosion area and the corrosion area. When the surface of the test piece is coated with eithe a less noble or a more noble metal than that of the matrix, its fatigue strength is recovered. The effects of different materials, test liquids and distances between the disc and test piece are also considered.

# I. Introduction

Some components exposed to cavitation erosion, such as hydraulic machinery, ship propellers and pumps, have often been fractured by the joint action of erosion and alternative mechanical stress. For instance, fatigue cracks in a hydraulic plunger pump quickly propagate from cavitation erosion pits around the plunger hole where the alternating stress activity is concentrated.[1] In this case, one of the causes is considered to be that the fatigue strength of the material was lowered due to the stress concentration at the bottom of the erosion pits which were formed by the fall-off of erosion particles. In other cases, electrochemical actions in both components and atmosphere are increased by the relative flow of corrosive liquid, the growth of cavitation bubbles, the increase of dissolved oxygen due to the incorporation of air, activation of the damaged surface, higher temperature of the liquid used, etc.

In general, corrosion is accelerated due to the presence of dissolved oxygen in the liquid. Furthermore, if areas of different oxygen concentrations develop in the liquid, an oxygen concentration cell is likely to be created such that the area of higher concentration is a cathode and the area of lower concentration is an anode. A temperature difference in the liquid will probably also create a thermo-galvanic cell. In the case of cavitation erosion in an atmosphere of larger electrical conductivity, an electrochemical cell is formed between an

eroded area and an uneroded area, and the corrosion is accelerated in the latter part. Therefore, we have to consider the corrosion fatigue strength of both the eroded part and the uneroded part around it.

In this report, torsional fatigue tests are carried out on steel bar specimens, which are exposed partially to cavitation in salt water or in ion-exchanged water, and the mutual relation between erosion and fatigue is made clear mechanically and electrochemically.

In addition, in order to increase the corrosion fatigue strength of the materials under cavitation erosion, it is very effective to protect the surface of the corrosion zone around the erosion zone by some suitable method. In this paper, fatigue tests under cavitation erosion are also carried out on specimens where the steel surface is plated with either a less noble metal or a more noble metal than itself, and the results of such plating is considered as well.

## II. Testing Apparatus and Test Procedures

Figure 1 shows a schematic view of a testing apparatus, which consists of a 4 kilogram-meter Schenk-type torsional fatigue tester, a magnetostrictive oscillator used for the cavitation erosion test and a cooling bath to keep the temperature constant. A piece of carbon steel of 0.35%C(S35C) is the main test material used, along with carbon steel of 0.55%C (S55C) and 18-8 stainless steel (SUS 304). The chemical compositions

of these materials are listed in Table 1. The shape and dimensions of the fatigue test piece are shown in Fig. 2. The heat treatment used before and after the manufacturing process and the mechanical properties of these test pieces are listed in Table 2. In addition, some S35C steel test pieces are plated on the surface with molten zinc and molten tin, respectively, the latter being first plated with molten copper. The thickness of the plating metals is approximately 20 microns in zincification and approximately 10 microns in tinning.

The test pieces are set parallel in water and held a small distance away from the disc surface, which is screwed into the free end of the amplifying horn of an oscillator, and alternative torsional stress is applied by the fatigue tester. The frequency of this fatigue tester is 1200 cycles per minute. The shape of the disc is shown in Fig. 3. The testing surface of the disc is polished with #2000 emery paper. The material of the disc is 18-8 stainless steel having a high resistance to cavitation erosion. However, as the disc is eroded by cavitation in long fatigue tests, the disc is exchanged with a new one after a single test. When this disc is screwed into the free end of the amplifying horn, the resonance frequency of the oscillator is 21.5 KHz.

The double amplitude of the free end of the disc is measured by a reading microscope in the air. These amplitudes are nearly proportional to the output current of the oscillator, and they are kept constant during the tests by controlling the currents.

Test liquids used are ion-exchanged water (specific resistance over 5 x $10^6 \Omega \cdot$cm) and 3% salt water (which is made by adding 3 weight-percent of salt to ion-exchanged water.) The water temperature is kept at 25° C and circulates at 2.8 l/min between the container and the electronic cooling bath.

The distance h between the disc and the fatigue test piece is h=0.5mm under conventional tests, with special instances where h=0.25, 1.0, 5.0, or 10.0 mm. As erosion damage to the fatigue test piece is affected by the distance h,[2][3] this h is measured with the dial gauge shown in Fig. 1. The testing surface of the disc is immersed to a depth of 3~4 mm from the water surface, which is kept level by the weir in the container.

## III. Experimental Results and Discussion

### III.1 The fatigue strength under cavitation erosion in salt water

To clarify the fatigue failure under cavitation erosion, a test is carried out where cavitation and alternative torsional stress act jointly on a test piece of 0.35% carbon steel in 3% salt water, under conditions where the distance h between the vibrating disc and the fatigue test piece is 0.5mm and the double amplitude $A_0$ of the disc end is 30 microns. The relation between the number of stress cycles N required to induce fracture and the torsional stress amplitude $\tau_a$ is shown in Fig. 4 (notation E.F.). The relation $\tau_a$-N under corrosion in 3% salt water (notation C.F.) and that in air

is also shown in Fig. 4.

At a large stress amplitude with less than $10^6$ cycles, the fatigue strength is not affected by cavitation erosion. However, at a smaller stress amplitude with more than $10^6$ cycles, the fatigue strength under cavitation erosion decreases more markedly than that under corrosion.

The fatigue strengths at $10^7$ cycles are 17.0 kg/mm$^2$ (24,200 psi) in the air, 11.5 kg/mm$^2$ (16,400 psi) under corrosion in 3% salt water, and 8.0 kg/mm$^2$ (11,400 psi) under cavitation erosion in 3% salt water. That is, the fatigue strength under corrosion is decreased by 32% from that in the air, and that under cavitation erosion by 53%. Under cavitation erosion, however, the fatigue fracture of test pieces occurs near the fillet, in the corrosion area outside of the erosion area. The stress concentration at the fillet is 1.06, much smaller than that at the bottom of either the erosion pit or the corrosion pit. Therefore, the remarkable decrease of the fatigue strength under cavitation erosion is considered to be due to the acceleration of corrosion in the corrosion area.

### III.2 The feature of erosion damage and fatigue crack propagation

An example of a test piece as it appears after the erosion fatigue test is shown in Fig. 5(a). The erosion damage occurs on the surface of the test piece within an elliptical area with a major axis of about 18mm, due to the cavitation generated by vibrating the disc. However, the area of about 2mm in width that forms a ring around the erosion area offers great

resistance against erosion and corrosion. Thus, the test piece surface may be broadly divisible into an erosion area (I), an area of corrosion resistance (II), and a corrosion area (III).

Figure 5(b) shows the front and back surface profiles of the test piece, with readings taken down a center line following the major axis. On the front, the side facing the disk, the surface roughness is greatest in the erosion area, while the surface of the corrosion resistance area is almost the same as the virgin surface. On the back, or the side facing away from the disc, the surface roughness is greater near the fillet than at the central part of the test piece.

Figure 6 shows the relationship of N (the number of stress cycles under torsional stress amplitudes $\tau_a = 12.0$ kg/mm$^2$ (17,100 psi 1) the depth of the maximum pit itself, and 2) the distance from the virgin surface to the tip of the maximum depth of erosion The maximum depth of the corrosion pit remains constant at about 20$\mu$m at more than $N=10^5$ cycles, but the depth of the eroded area continues to increase with the number of stress cycles. The maximum erosion pit depth at $N=2.98 \times 10^6$, when fracture occurs, reaches twice the depth of the maximum corrosion pit. The maximum distance from the surface, moreover, comes to about six times that in the case of corrosion.

The distribution of crack lengths at the cross section along the major axis of the test piece is shown in Fig. 7. The number of these cracks is greater at the erosion area than at the corrosion area, but the crack lengths of the former are shorter. For

example, the maximum crack lengths in the corrosion area and in the erosion area are plotted in Fig. 8 against the number of stress cycles under $\sigma_a = 12$ kg/mm$^2$ (17,100 psi). In the early stages, the crack in the corrosion area deepens gradually with the increase of the number of stress cycles until it reaches about 1mm in length. After that it propagates very rapidly and eventually gives rise to a fracture in the test piece. On the other hand, from the outset the cracks in the erosion area reach only half the length of the corrosion-area cracks, and they hardly propagate even with increase of stress cycles. Figure 9 shows an example of cracks at the tips of erosion pits and corrosion pits. The crack in the corrosion area propagates farther in the radial direction, but the cracks in the erosion area grow only slowly even with a large number of stress cycles, and as they propagate in various directions erosion particles fall off from the surface.

Figure 10 shows the micro-Vickers hardness below the tips of erosion pits and corrosion pits. These hardnesses are measured along the radial direction of the test piece only at the ferrite matrix etched with 3% nital. The bottom of the erosion pits has a larger work-hardening layer than that of corrosion pits, and its depth reaches 1-2mm.

### III.3 Galvanic cell formation

It can be considered that a galvanic cell is formed between the erosion area and the corrosion area by differences of temperature, dissolved oxygen concentration, ion concentration,

speed of liquid flow, materials, etc. The corrosion potential of the test piece surface is measured with a calomel half-cell as a reference half-cell under test conditions of $\tau_a$ = 12.0 kg/mm$^2$, h=0.5mm; the resulting distribution is shown in Fig. 11. A potentiometer with input resistance larger than 1000 MΩ is used, and the tip of the Luggin capillary of the electrode is closed about 0.2mm away from the surface to be measured. However, since the potential of the eroded surface cannot be measured directly, readings are taken along the side and the back, down the major axis, at intervals of 5mm. (17,10

During the initial period of erosion, as shown in Fig. 11(a), the potential of the side is about 10mV higher than that of the back, but both potentials remain fairly constant in the direction of the generation. During the development stage, as shown in Fig. 11(b), the potential of the place close to the eroded area is higher. It is considered that a galvanic cell is formed such that the erosion area becomes a cathode and the corrosion area an anode. Also, as shown in Fig. 12, the test piece is cut at a point about 10mm from the center and is annealed in a vaccum. After that, the shorter of the two pieces is coated with insulating paint except for a band 8mm wide, and the other larger piece is coated except for the eroded surface area. The separation between the two cut surfaces is closed to about 1 mm; the shorter piece is connected with the (+)terminal of the potentiometer and the larger piece with the (-)terminal. Before the cavitation test is carried out the potenti

is zero, but under the cavitation conditions of h=0.5mm and $A_0$=30μm it reads + 50mV. On the other hand, when the galvanometer is used instead of the potentiometer, the corrosion current gives + 0.45-0.50mA. Converted to current density this becomes about 0.2mA/cm$^2$. This value is very large in comparison with the less than 5μA/cm$^2$ value of low carbon steels in 3% salt water.[4]

Consequently, the decrease of fatigue strength under cavitation erosion is caused by the accelerated corrosion of the corrosion area. On the other hand, the fatigue strength of the erosion area is expected to increase, so that the erosion area becomes more cathodic, a larger work-hardening is formed at the bottom of the erosion pits, and crack propagation is slowed (as made clear in the previous chapter.)

### III.4 The effect of h

As the cavitation intensity depends on the distance h,[2],[3] changing h may affect the relation between the fatigue strength and the erosion rate. Thus similar fatigue tests are carried out with h=0.25 mm and h=0.50 mm. Figure 13 shows the S-N curves under corrosion and under erosion with H=0.25, 0.5, and 5.0 mm. In the low stress range of more than N=10$^6$, the fatigue strength under erosion decreases more than that under corrosion for all values of h. As illustrated in Table 3, the fracture of all test pieces occurs at the corrosion area. The size of the erosion area under h=0.5mm almost agrees with that under h=0.25mm, but the erosion area under h=0.5mm is half the size of the former

and its area is not clearly separated from the corrosion resistance area. With increased h the macro-galvanic cell caused by cavitation erosion is hardly formed, although the corrosion caused by the local-action cells may be accelerated due to the liquid flow and the increase of dissolved oxygen in the testing liquid. Thus when h is small fracture occurs consistently at the fillet. However, when h is large, the fracture points are scattered throughout the area and fracture may occur even near the middle of the test piece. But the relation between the fatigue strengths of the erosion area and of the corrosion area cannot be clarified from Fig. 13.

The hardness and the cracks of a cross section of the test piece are observed after the fatigue test run under the test conditions of $\tau_a$= 12.0 kg/mm$^2$, (17,100 psi) h=0.25mm and $\tau_a$=12.0 kg/mm$^2$, h=5.0mm. Figure 14 shows the distribution of hardness measured in a radial direction from the tip of the pits in the erosion area. The hardness of the corrosion surface is not changed by h, similarly to what was shown in Fig 10(b), but the hardness of the eroded surface increases extremely in the case of smaller h. Figure 15 shows the crack initiation points and the crack lengths. Under h=0.25mm, the cracks propagate deeply in the corrosion area near the fillet. However, under h=0.5mm, comparatively large cracks are observed even at the erosion area. When h becomes larger, the cracks propagate easily even in the erosion area because of the decrease of the fall-off of the erosion particles. That is, the fatigue strength at the erosion

area must be considered to increase rather than decrease with an increase of cavitation intensity.

### III.5 Fatigue strength in ion-exchanged water

Figure 16 shows the results of fatigue tests run on S35C test pieces in ion-exchanged water, in particular under the test conditions of a double amplitude $A_0$ 35μm and the distances h=0.25mm, 0.5mm, 1.0mm, 5.0mm, and 10.0mm. In the high stress range of less than $N=10^6$, the effect of the cavitation on the fatigue strength is slight. However, in the lower stress range of more than $N=10^6$, the E.F. strength increases more than the C.F. strength at the same stress cycle, in contrast with the result in salt water. This tendency is more remarkable the smaller the distance h is.

The appearance of the surface of the test pieces is similar to that in salt water, discussed in the preceding sections. All the fracture points of the test pieces, as illustrated in Table 5, are clustered at the corrosion area, except in the case of h=5.0mm. Consequently, this result, shown in Fig. 16, means that the fatigue strengths of both the erosion area and the corrosion area increase. It is thought that the surface of the test piece is quickly passivated with the increase of dissolved oxygen in liquid because of the lack of $Cl^-$ ions in ion-exchanged water. On the other hand, the increase of the fatigue strength of the erosion area, as described in the previous section, is considered to be caused by the fall-off of erosion particles and the work-hardening of the erosion surface.

The fracture at the eroded area under h 5.0mm, however, is due to the fact that, as shown in Fig. 17, a relatively deep pit is formed at the center of the eroded area and leads to fracture. It is reported that a small number of deep local cracks is caused when the cavitation intensity is small.[5] This characteristic property appears to explain the phenomenon that the fatigue strengt is smaller for h=0.5mm than for h=10.0mm, as shown in Fig. 16.

III.6 The effects of materials

Figures 18 and 19 show the S-N curves of 0.55%C carbon steel (S55C) and stainless steel (SUS 304), respectively. In the figures the asterisk* represents the test piece fractured at the erosion area. The surface of the S55C test piece is clearly divided into three areas, similar to S35C. That of SUS 304 can be divided into the erosion area(I) and the uncorrosion area (II), with no corroded area even at $n=10^7$. These erosion areas form an ellipse with a major axis of about 18mm on both materials, but the depth of erosion differs. When they are compared under the same test conditions, as illustrated on Table 5, the erosion resistance under the alternative stress is higher on S55C and SUS than on S35C.

The nature of S55C material is to have high erosion resistance but it easily forms a galvanic cell so that it is easily corroded. It also has a large notch sensitivity. Thus, the fracture always occurs at the corrosion area and, on the whole, the fatigure stren under erosion is lower than that under corrosion. On the other ha

SUS 304

material does not form a galvanic cell due to cavitation erosion, for it has much higher erosion resistance as well as being a passivitation metal. So in the low stress range the fatigue strength under erosion decreases more than that under corrosion, and the fracture occurs at the erosion area because erosion damage is greater than corrosion. In the high stress range, where the test piece undergoes extreme increase of heat due to the repeated stress, the fatigue strength is higher under erosion than under corrosion. This is due to the greater cooling effect in the erosion area by the cavitation liquid flow. In this case, the fracture point belongs near the fillet where the cooling effect is bad.

III.7 The fatigue strength of plated test pieces.

Figures 20 and 21 show the S-N curves of test pieces plated with molten zinc and molten tin, respectively. In addition, the results of Fig. 4 are also shown by a dotted line and a chained line. In Fig. 20 the fatigue strength of the zincified test piece/under corrosion decreases with N but it is larger than the corrosion fatigue strength of a normal (unplated) test piece at $N=10^7$. Moreover, the /corrosion fatigue strength under the double amplitude $A\sigma=35\mu m$ differs little from that under ~~double~~ $A\sigma=20\mu m$ in the high stress range, though the strength of the former decreases more remarkably than that of the latter in the low stress range. In the long run, the fatigue strength of the zincified test piece/under cavitation erosion approaches the erosion fatigue strength of normal test piece after about $n=5 \times 10^6$ for $A\sigma=35\mu m$ and after

a somewhat larger number of stress cycles for Ao=20um, due to the different rates at which the plated zinc is dissolved.

In Fig. 21, the corrosion fatigue strength of the tinned test piece is shown to be almost the same as the corrosion fatigue strength of a normal test piece. The fatigue strength of the tinned test under cavitation erosion is lower than either of these corrosion fatigue strengths and decreases with N, but it does not reach the even lower fatigue strength of the normal test piece under cavitation erosion. Whether the plated metals are more noble or less noble than the matrix, then, plating is one effective method for increasing the fatigue strength of material components on which cavitation erosion occurs.

III.3 Crack propagation in plated test pieces.

This section will consider the various surface phenomena that occur on the test pieces as brought forward in the previous sections.

The normal test piece fractured in a zigzag across the surface perpendicular to the major axis because the many cracks which occur around the piece at this position connect. However, in the corrosion fatigue of the plated test pieces, as shown in Fig. 22, the cracks propagate in the principle stress direction, and two cracks crossing in an X lead to fracture. The cracks in the zincified test piece propagate quickly after crack initiation, and lead to fracture. The cracks in the tinned test pieces propagate more slowly. In other words, the crack propagation of the zincified test piece in water shows tendencies similar

to that of a normal test piece in the air, since the cathodic protection due to zincification keeps the matrix from corroding. In the tinned test piece, a local corrosion cell with the tinning layer acting as cathode and the matrix as anode is formed at defects such as pinholes, so that the tips of the cracks are dissolved. Thus the cracks propagate slowly.

Some examples of the surfaces of plated test pieces after fatigue test runs under cavitation erosion are shown in Fig. 23. An elliptical area with a major axis of about 16mm is quickly eroded by cavitation and the plating layer is broken down. Moreover, in the zincified test piece, a corrosion resistance area in the form of a ring of 1-2mm width appears around the eroded area, but the surface of the ring area is the base matrix because the zinc layer is dissolved. The zinc layer adjacent to the ring area is also gradually corroded with the increase of the test duration. When the zinc layer is entirely dissolved, the effect of the sacrificial anode is lost and red rust appears on the surface of the matrix. On the tinned test piece, a copper band around the elliptical area appears as the corrosion resistance area. Furthermore, another band of 1-2 mm width around the copper layer is remarkably corroded. Outside this area, the tin layer remains complete and protects the matrix.

The area of the crack growth related to the fracture of the zincified test piece differs between cycles of more and less than $N=5 \times 10^5$. In the higher stress range, one crack, or two cracks in an X, originate at the point within the erosion area that is farthest from the disc, and propagate quickly.

In the lower stress range, many cracks grow at the point of minimum distance from the disc and propagate from the corrosion area through the corrosion resistance area in a zigzag perpendicular to the major axis of the test piece. On the other hand, in the tinned test piece, many cracks grow at severely eroded places in the far edges of the eroded area and at many places in the corrosion area outside of the copper layer, and some of these cracks propagate in the principal stress direction. The propagation rate is slower, particularly in the erosion area, and one of these cracks leads to fracture.

Figure 24 shows: 1) the mean distance from the virgin surface to the erosion surface; 2) the maximum distance from the virgin surface to the erosion surface; and 3) the depth of the maximum pit itself (actually the mean value of the three largest pits' depths). All of these values are measured in the direction of the major axis of the test piece by a surface profilometer, beginning at the position closest to the disc and rotating the line of measurement by units of 10 degrees around the curved surface. Table 6 also shows the depth of the maximum pit itself (again calculated as above) for the fractured test pieces of Fig 20, at the position of minimum distance to the disc and at a second position rotated by about 35 degrees from the first.

In general, when the distance from the disc is small, new erosion particles fall off continuously and erosion damage is severe. On the other hand, when the distance from the disc

is large, the cracks made by collapse pressure propagate more deeply because the work-hardening layer is hardly formed, and large pits are created. But erosion damage is slower. Therefore in the higher stress range the fatigue cracks originate more easily at the position of greater distance from the disc than at the minimum distance. However, at more than about $N \fallingdotseq 5 \times 10^6$, the test duration time is long and the minimum distance becomes larger than it was originally, due to the increase of erosion damage. Then large pits are formed even at the point of minimum distance, and the fatigue cracks propagate easily. With even longer test duration the zinc layer dissolves completely, corrosion pits are formed, and fracture occurs even in the corrosion resistance area. Consequently, the behavior of these fatigue cracks is related to the fatigue strength of the plated specimens shown in Figs. 20 and 21.

## IV. Conclusion

To clarify the effect of cavitation erosion on fatigue strength, fatigue tests have been carried out in 3% salt water and ion-exchanged water. The results obtained are as follows:

(1) In the case of S35C and S55C carbon steel in 3 salt water, the fatigue strength under cavitation erosion decreases more than the corrosion fatigue strength , as explained in (2) below, but fracture of the former also occurs in the corrosion area outside of the erosion area.

(2) The fatigue strength of the corrosion area in the fatigue test under cavitation erosion decreases more than that in the case of corrosion fatigue, due to the macro-galvanic cell formed between the corrosion area and the erosion area. On the other hand, the fatigue strength of the erosion area increases due to the formation of a thick layer of work-hardening and to the interference of erosion particle fall-off in crack propagation at the bottom of the erosion pits.

(3) In the case of ion-exchanged water, the fracture of the test pieces occurs, similarly, at the corrosion area, except in a few cases, but the fatigue strength under cavitation erosion increases more than the corrosion fatigue strength. This is because the surface of the test piece is quickly passivated due to the increase of dissolved oxygen in the liquid from cavitation activity, and because the fatigue strength of the erosion area also increases as explained in (2).

(4) In the case of SUS 304 stainless steel, the fatigue strength under cavitation erosion increases more than the corrosion fatigue strength in the high stress range and the fracture of the test pieces occurs at the periphery where the influence of cavitation flow is slight. In the low stress range, however, the fracture occurs in the erosion area due to the damage of cavitation erosion and the fatigue strength under erosion decreases more than the corrosion fatigue strength.

(5) When the surface of the test piece is coated with

either zinc, a less noble metal, or tin, a more noble metal than that of the matrix, the E.F. strength increases more than that of a normal test piece. That is, plating is one effective method for increasing the fatigue strength of material components on which cavitation erosion occurs.

Acknowledgment

Sincere thanks are due to F. G. Hammitt, Professor of The University of Michigan and K. Endo, Professor of Kyoto University for their kind suggestions and discussions. Typing and reproduction supported by ONR Contract NOOO14-76-C-0697.

References

1) Kikai no Songai, 10-4 ( 1967 ), 94. ( in Japanese )

2) K. Endo et al: JSME, 32-237 (1966-5), 831.

3) T. Okada and Y. Nishimura: Memoirs of the Faculty of Engineering Fukui University, 19-1 (1971-3), 19. ( in Japanese )

4) Uhlig, H.H.(Matsuda and Matsushima; Translation); Corrosion and Corrosion Control, (1968), 85, Sangyotosho.

5) K. Endo and Y. Nishimura: JSME, 38-309 (1972-5), 924.

Table 1 Chemical compositions of fatigue test pieces

| Materials | C | Si | Mn | P | S | Cu | Ni | Cr |
|---|---|---|---|---|---|---|---|---|
| S 35 C | 0.37 | 0.24 | 0.74 | 0.011 | 0.026 | 0.08 | — | — |
| S 55 C | 0.54 | 0.27 | 0.82 | 0.016 | 0.017 | 0.02 | 0.02 | 0.09 |
| SUS 304 | 0.08 | 0.60 | 1.58 | 0.039 | 0.020 | — | 8.68 | 18.44 |

Table 2 Heat treatment and mechanical properties of fatigue test pieces

| Materials | Heat treatment | | Tensile strength kg/mm² | Elongation % | Reduction in area % | Hardness Hv |
|---|---|---|---|---|---|---|
| | Before Mfg. Process | After Mfg. Process | | | | |
| S35C | 880°C 1 h Normalizing | 600°C 30 min Annealing | 58 | 33 | 57 | 172 |
| S55C | 830°C 1 h Normalizing | 600°C 30 min Annealing | 66 | 28 | 46 | 210 |
| SUS 304 | 1 110°C Water quenching | —— | 60 | 67 | 72 | 334 |

Table 3 Fracture positions of S35C fatigue test pieces in 3% salt water

| | Flat surface | | | | Fillet |
|---|---|---|---|---|---|
| Distance from the center of test piece | 0~5 mm | 5~10 mm | 10~15 mm | 15~20 mm | 20 mm |
| CF | 0 | 0 | 3 | 5 | 0 |
| EF $h$=0.25 mm | 0 | 0 | 0 | 3 | 0 |
| EF $h$=0.5 mm | 0 | 0 | 2 | 10 | 0 |
| EF $h$=5.0 mm | 0 | 1 | 1 | 2 | 0 |

Table 4 Fracture positions of S35C fatigue test pieces in ion-exchanged water

| | Flat surface | | | | Fillet |
|---|---|---|---|---|---|
| Distance from the center of test piece | 0~5 mm | 5~10 mm | 10~15 mm | 15~20 mm | 20 mm |
| CF | 1 | 1 | 2 | 3 | 0 |
| EF $h$=0.25 mm | 0 | 0 | 1 | 3 | 0 |
| EF $h$=0.5 mm | 0 | 0 | 1 | 6 | 0 |
| EF $h$=1.0 mm | 0 | 0 | 1 | 4 | 0 |
| EF $h$=5.0 mm | 2 | 0 | 1 | 2 | 0 |
| EF $h$=10.0 mm | 0 | 0 | 2 | 4 | 0 |

Table 5 Maximum depth of erosion on every test piece in 3% salt water

| Materials | Stress amplitude $\tau_a$ kg/mm$^2$ | Fracture cycles number $N$ | Maximum depth of erosion $\mu$ |
|---|---|---|---|
| S35C | 12.0 | $2.27\times10^6$ | 125 |
| S55C | 〃 | $2.22\times10^6$ | 100 |
| SUS 27 | 〃 | $10^7$ No fracture | 150 |
| 〃 | 16.0 | $2.34\times10^6$ | 64 |

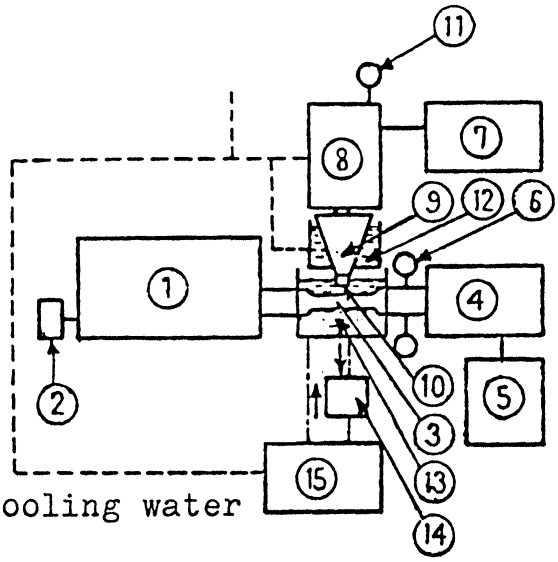


1 4 Kg-m Schenk type torsional fatigue tester
2 Revolution counter
3 Test piece
4 Stress measuring instrument
5 Recorder
6 Dial gauges to set up a stress
7 Ultrasonic generator
8 Magnetostrictive oscillator
9 Amplifying horn
10 Disc
11 Dial gauge to set up the distance between the disc and the test piece
12 Cooling bath of the horn
13 Container of test liquid
14 Filter
15 Electronic cooling instrument

Fig.1 Schematic view of a testing apparatus

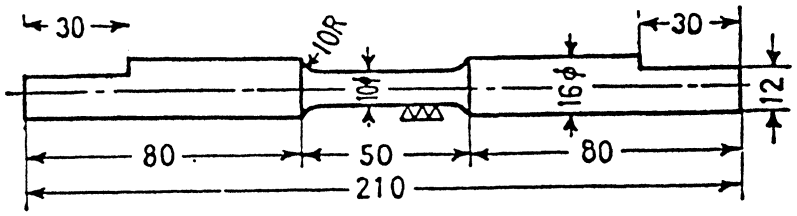


Fig.2 Shape and dimensions of fatigue test piece

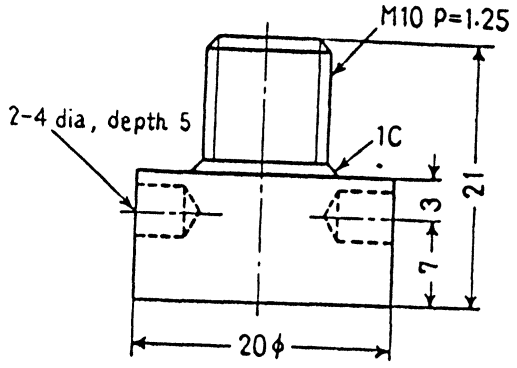


Fig.3 Shape and dimensions of disc

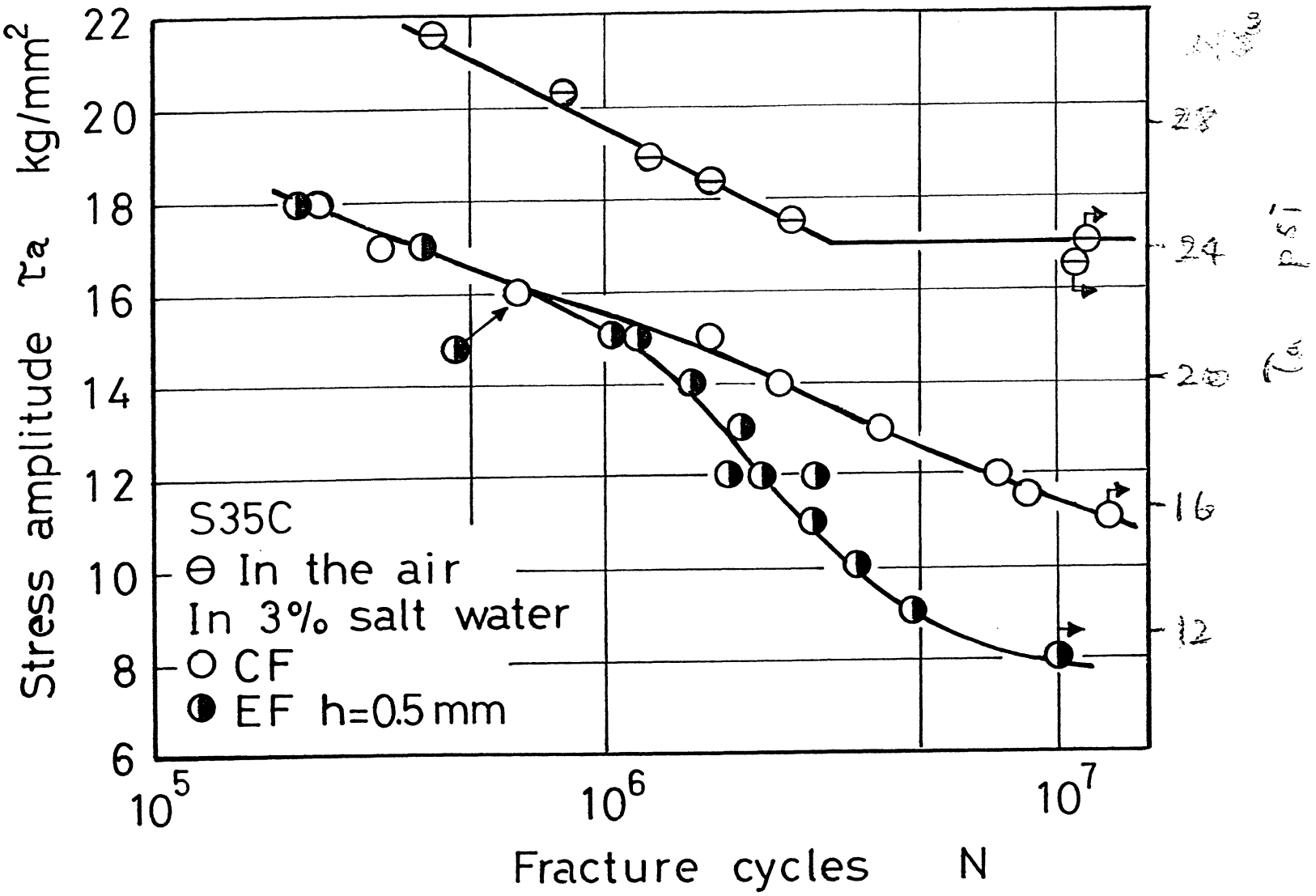


Fig.4 S-N curves of S35C fatigue test pieces in 3% salt water

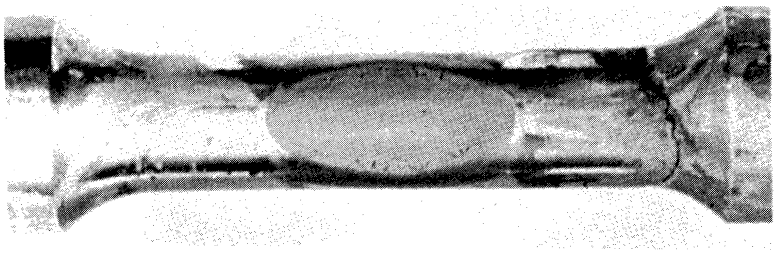

(a)

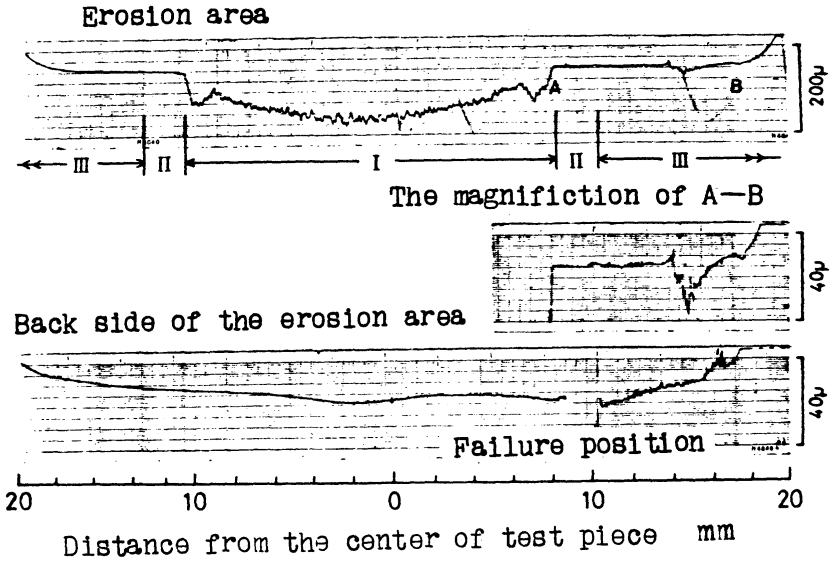


(b)

In 3% salt water, $\tau_a$=12.0 Kg/mm$^2$ , h=0.5 mm, N=1.95x10$^6$

Fig.5 Example of a test piece surface.

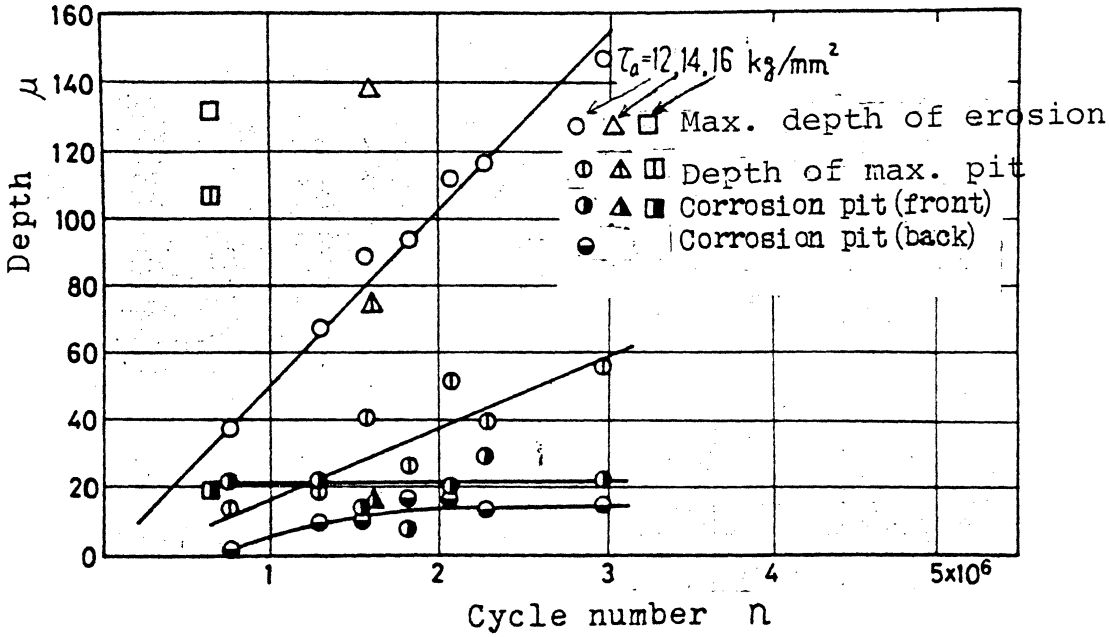


Fig.6 Depth of the maximum pit itself and distance from the virgin surface to the trip of the maximum pit (maximum depth of erosion)

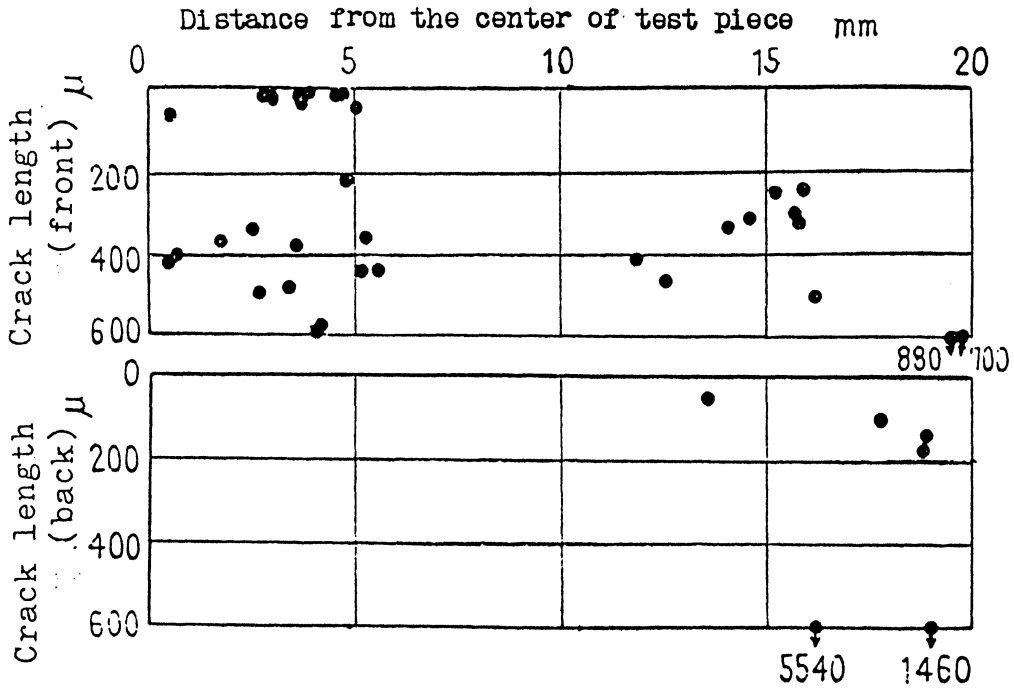


In 3% salt water, $\tau_a = 12.0\,\mathrm{kg/mm^2}$, $h = 0.5\,\mathrm{mm}$, $N = 2.98 \times 10^6$

Fig.7 Distribution of cracks

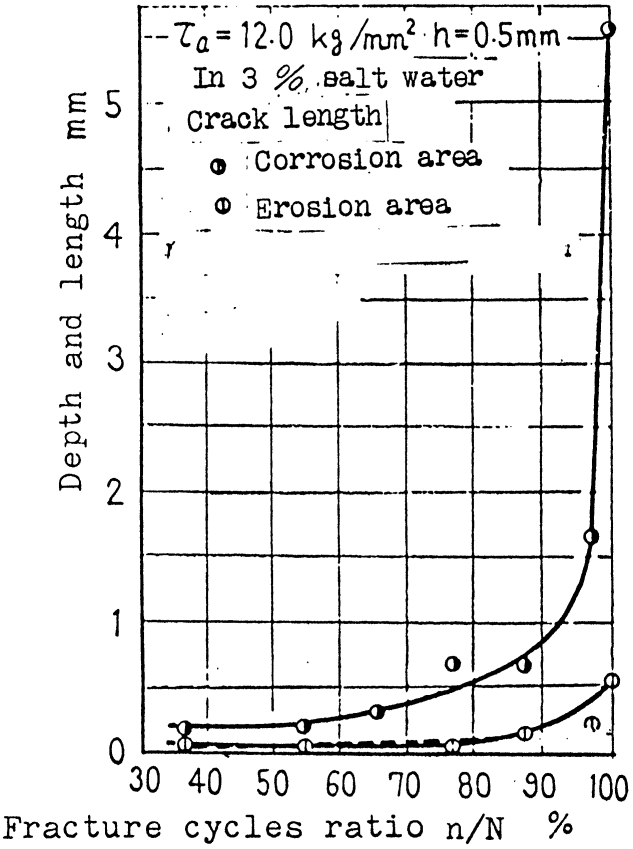


Fig. 8 Relation between the maximum crack length and the cycle number

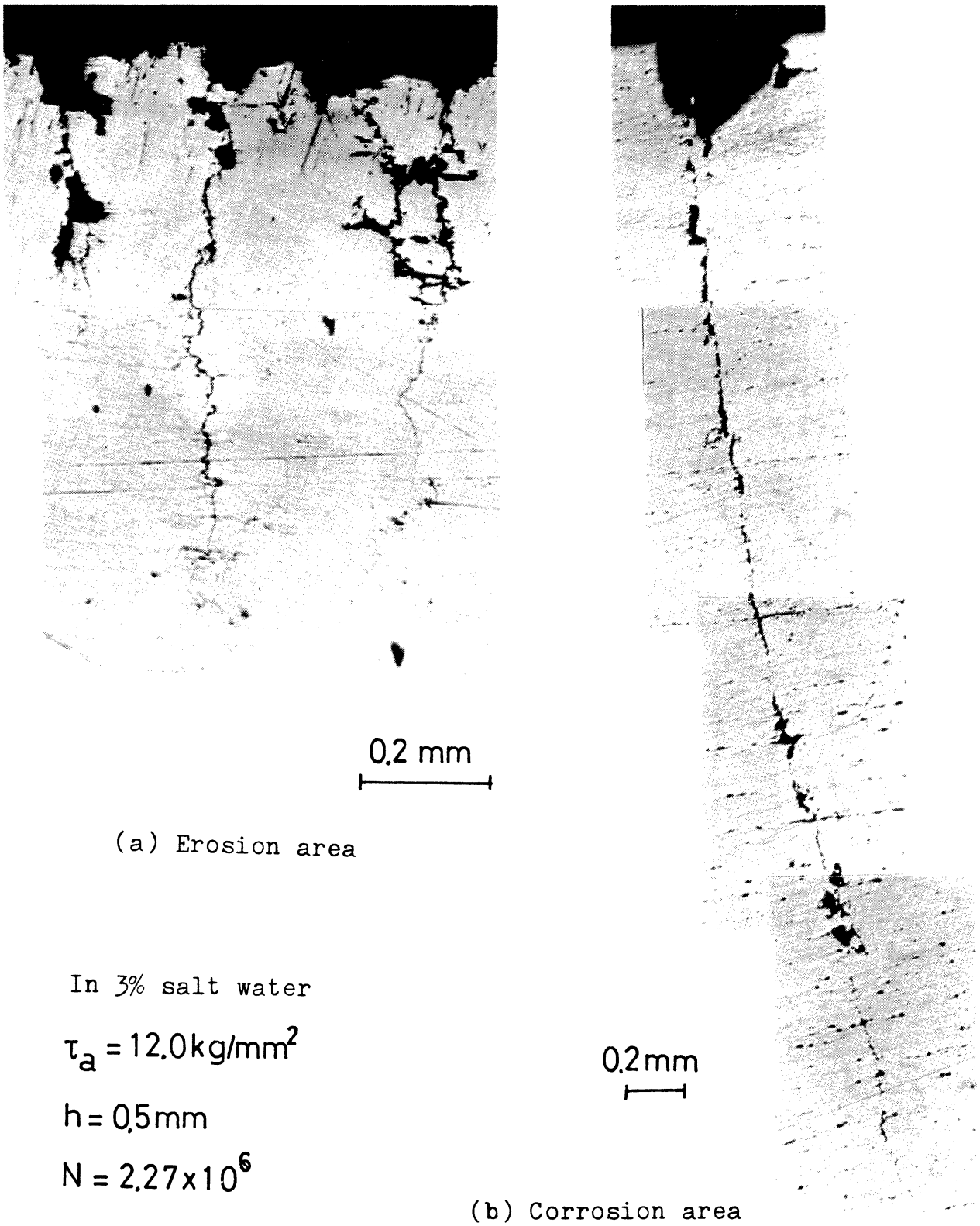


Fig.9 Examples of cracks

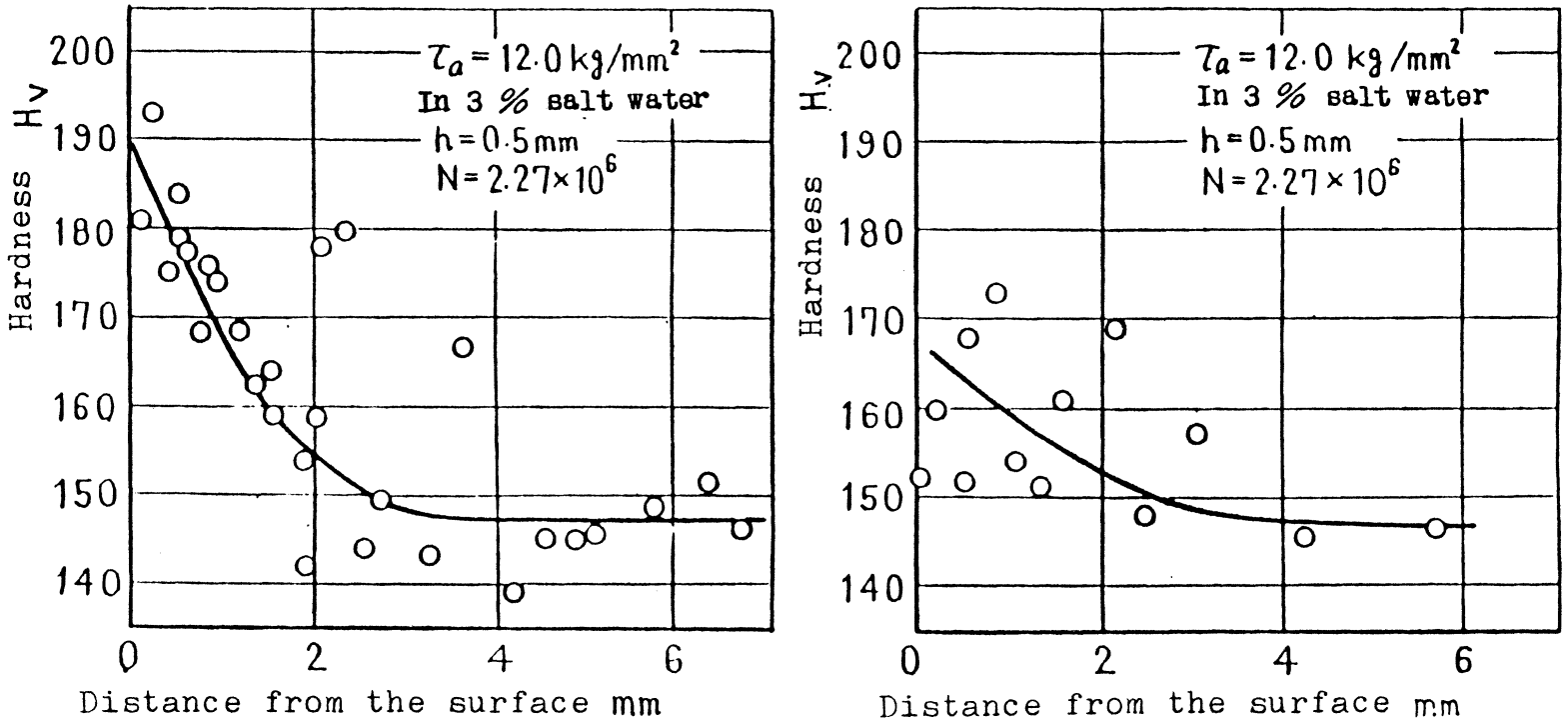


Fig.10 Distributions of hardness of pit bottoms

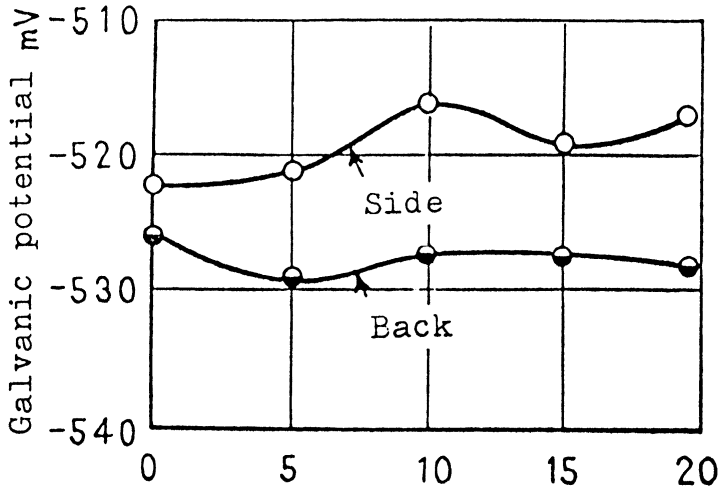


(a) After the start of test

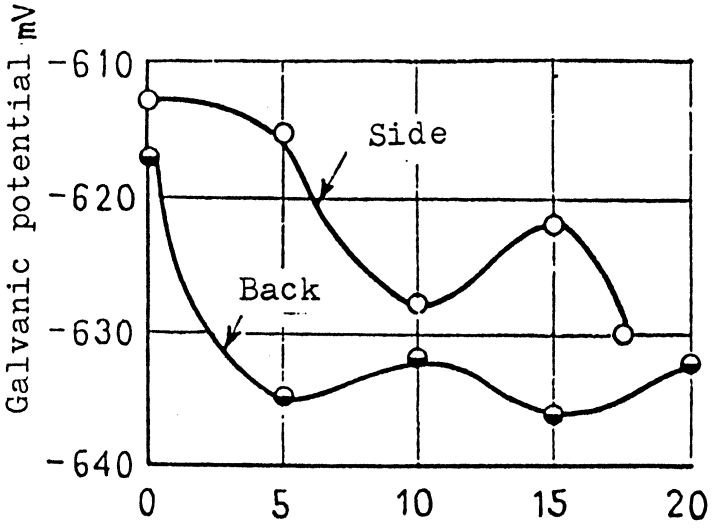


(b) $n=1.14\times10^6$ (15.8 h)

In 3% salt water, $\tau_a=12.0\,kg/mm^2$, $h=0.5\,mm$

Fig.11 Distributions of galvanic potential in test piece

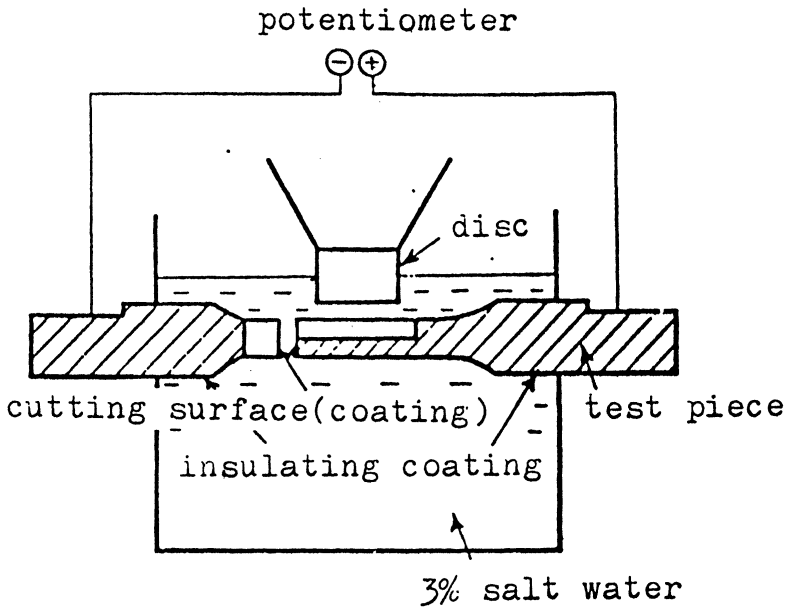


Fig.12 Measurement of potential between the erosion area and the corrosion area

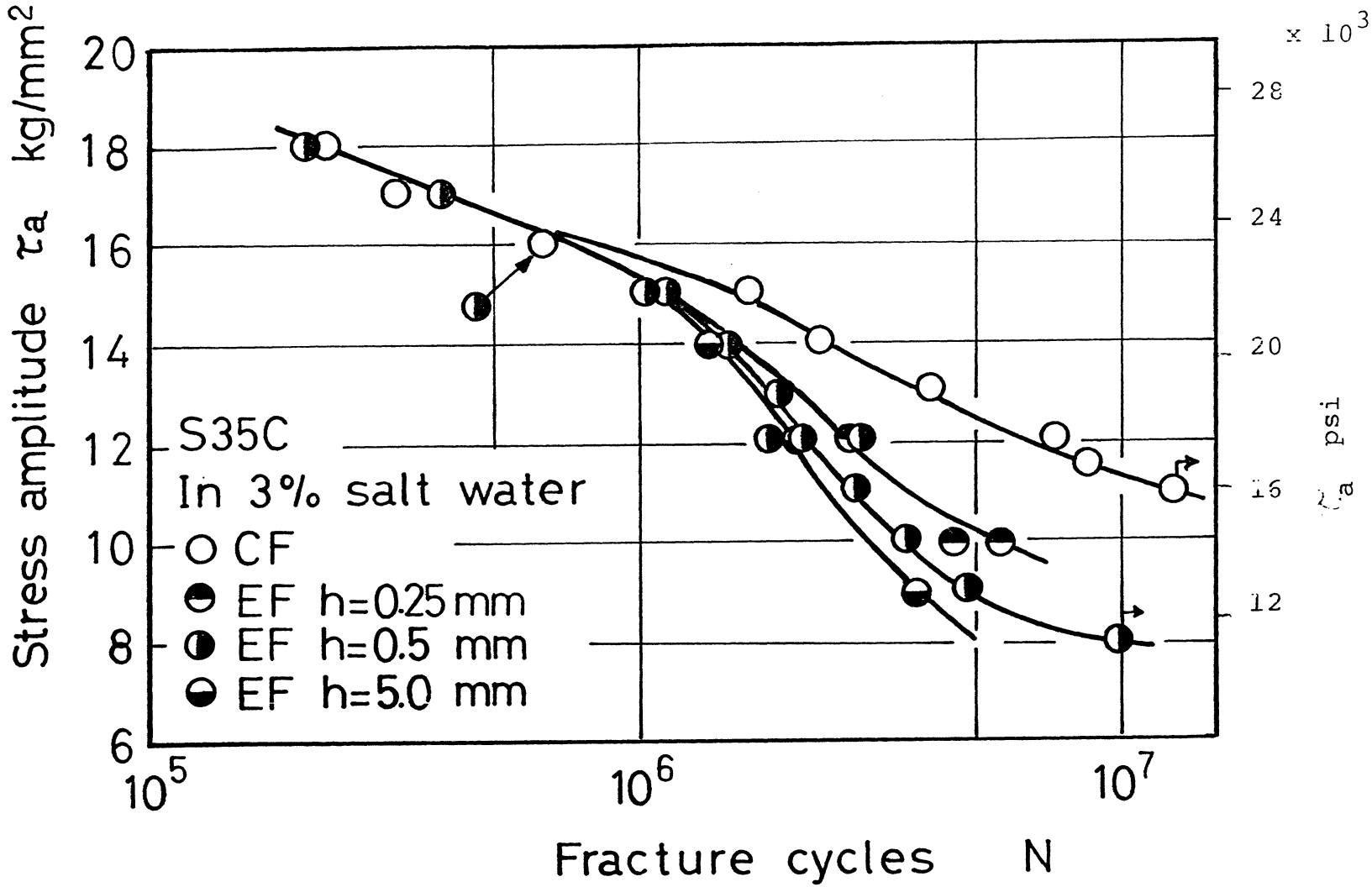


Fig.13 Effect of the distance h on the fatigue strength

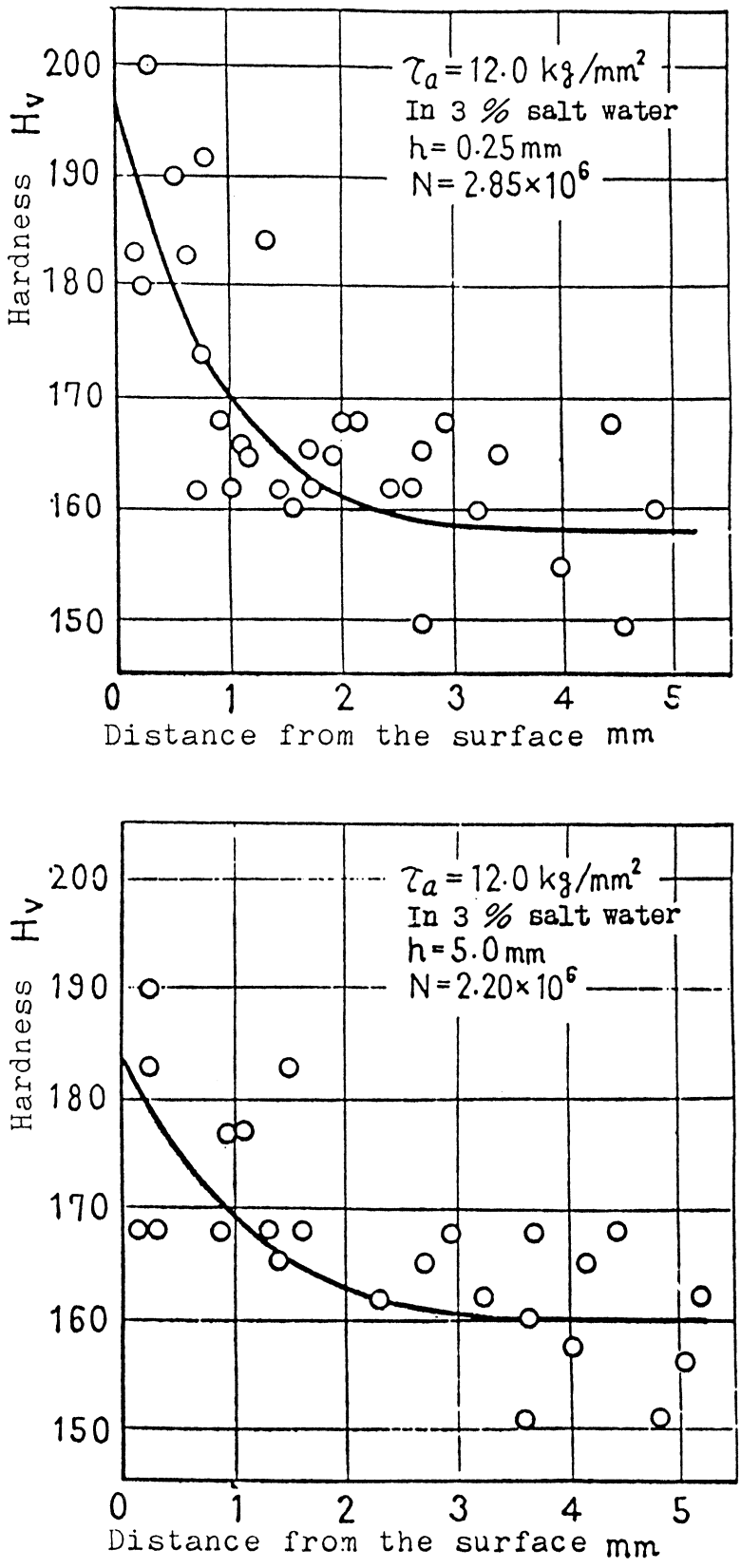


Fig. 14 Distribution of hardness of pit bottoms (in the erosion area)

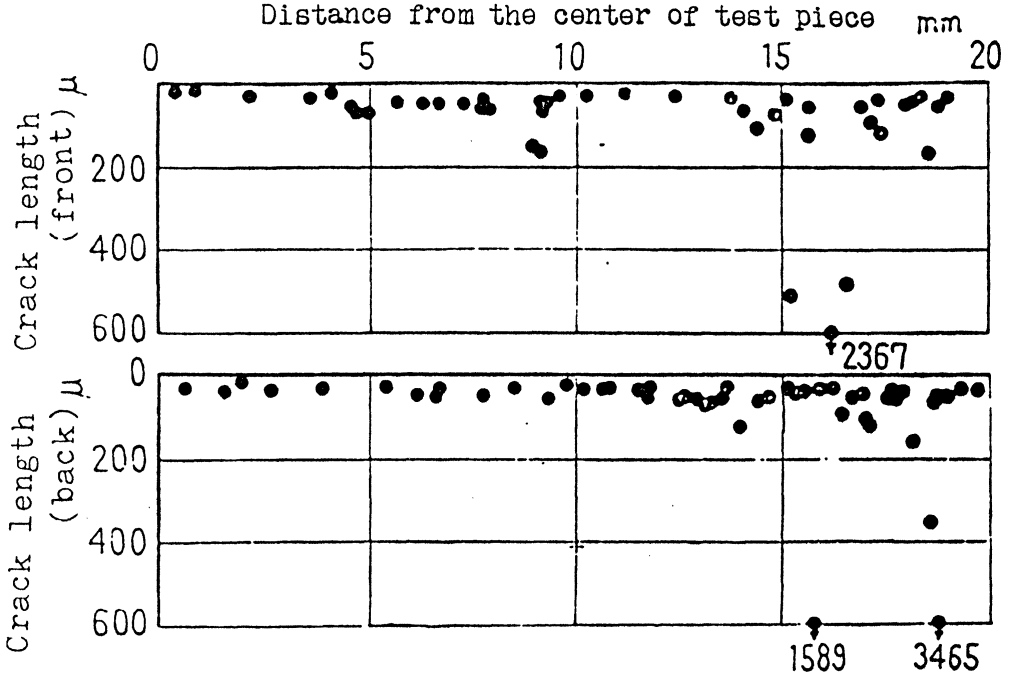


(a) In 3% salt water, $\tau_a = 12.0\,kg/mm^2$
$h = 0.25\,mm$, $N = 2.85 \times 10^6$

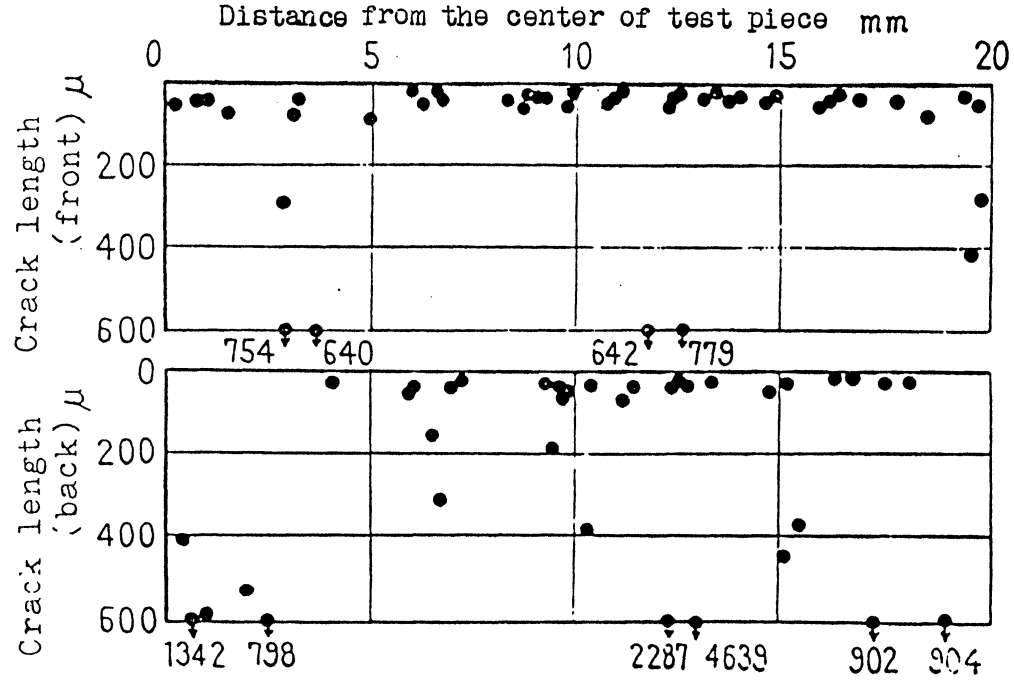


(b) In 3% salt water, $\tau_a = 12.0\,kg/mm^2$
$h = 5.0\,mm$, $N = 2.20 \times 10^6$

Fig.15 Distribution of cracks

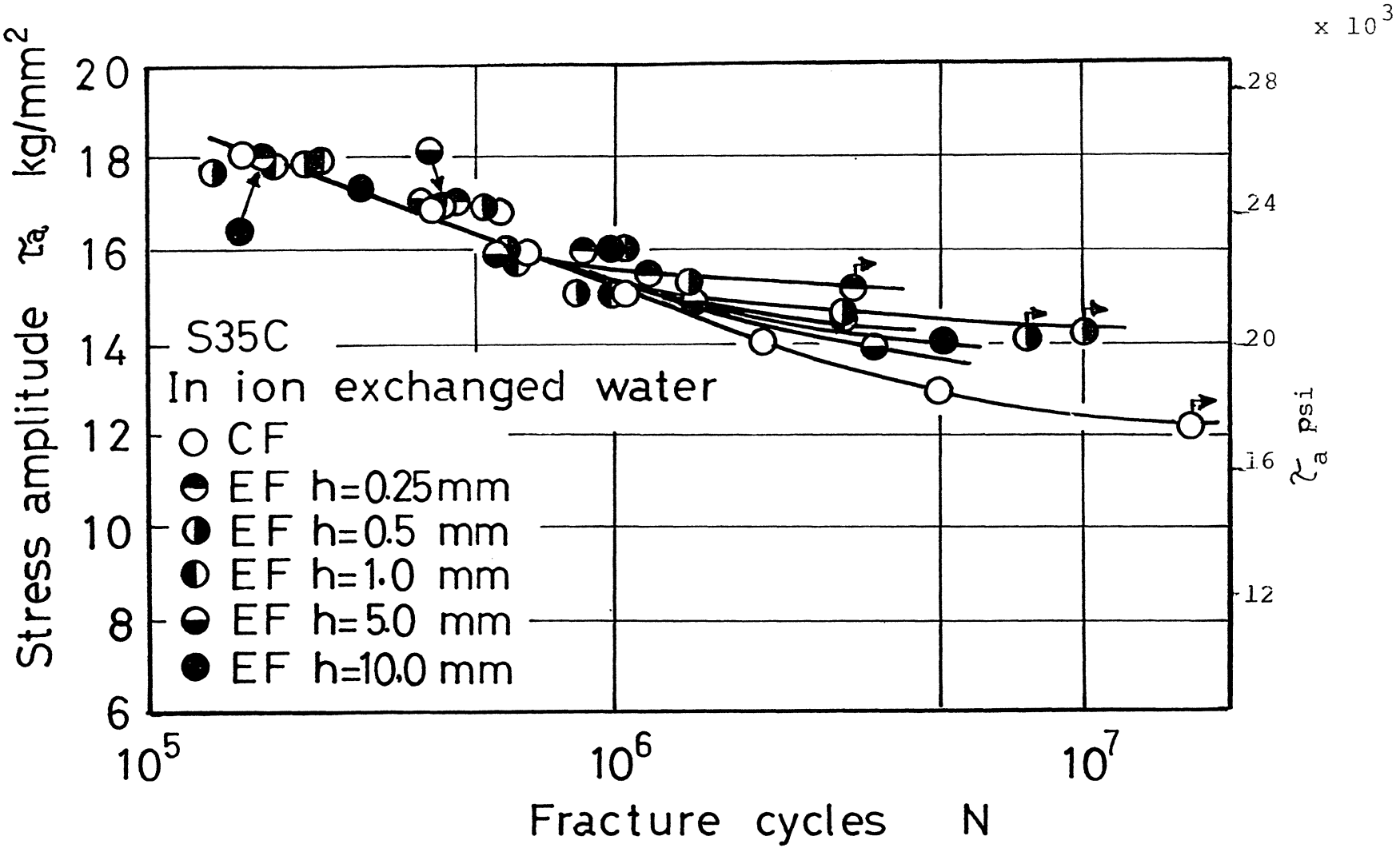


Fig. 16 S-N curves of S35C fatigue test pieces

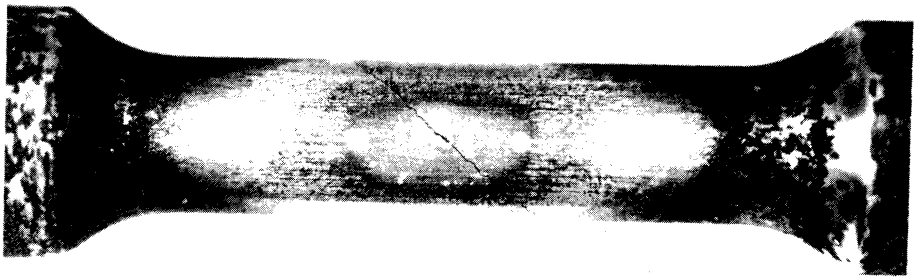

In ion-exchanged water,

$\tau_a = 14.0\ kg/mm^2$, $h = 5.0\ mm$,

$N = 4.54 \times 10^6$

Fig.17 Example of fracture in the erosion area

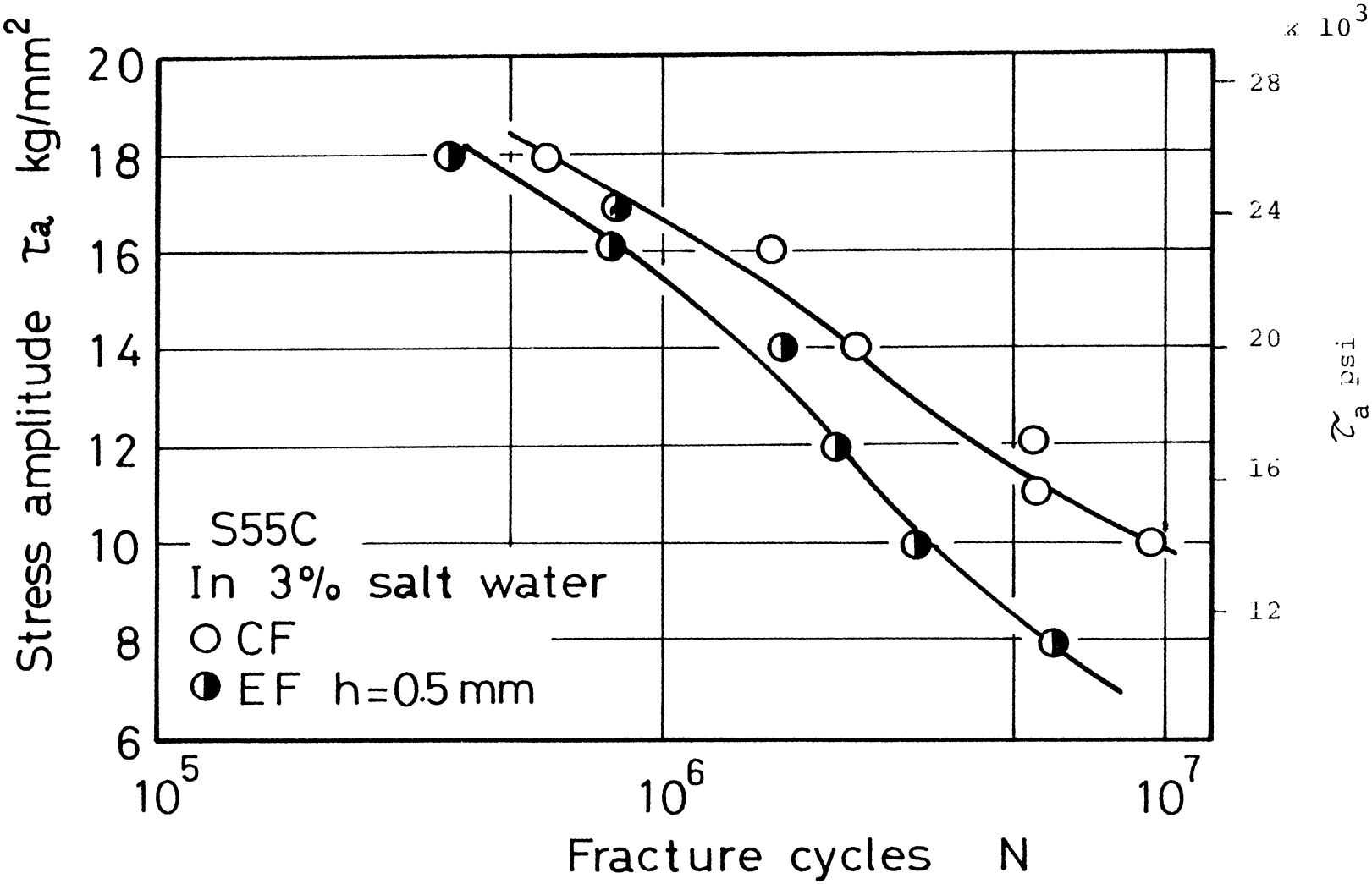


Fig.18 S-N curves of S55C

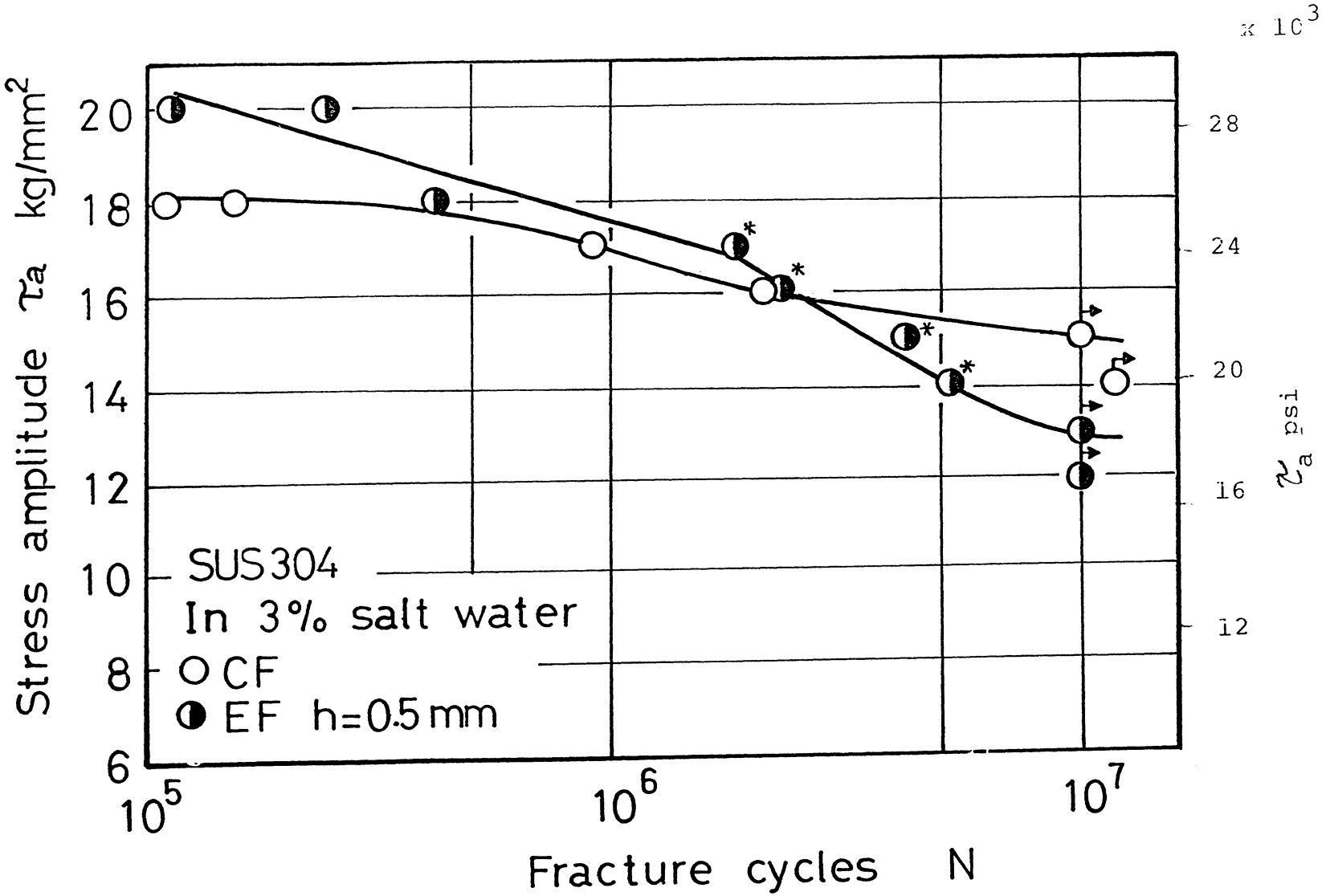


Fig.19 S-N curves of SUS304 fatigue test pieces in 3% salt water (*: fracture in the erosion area)

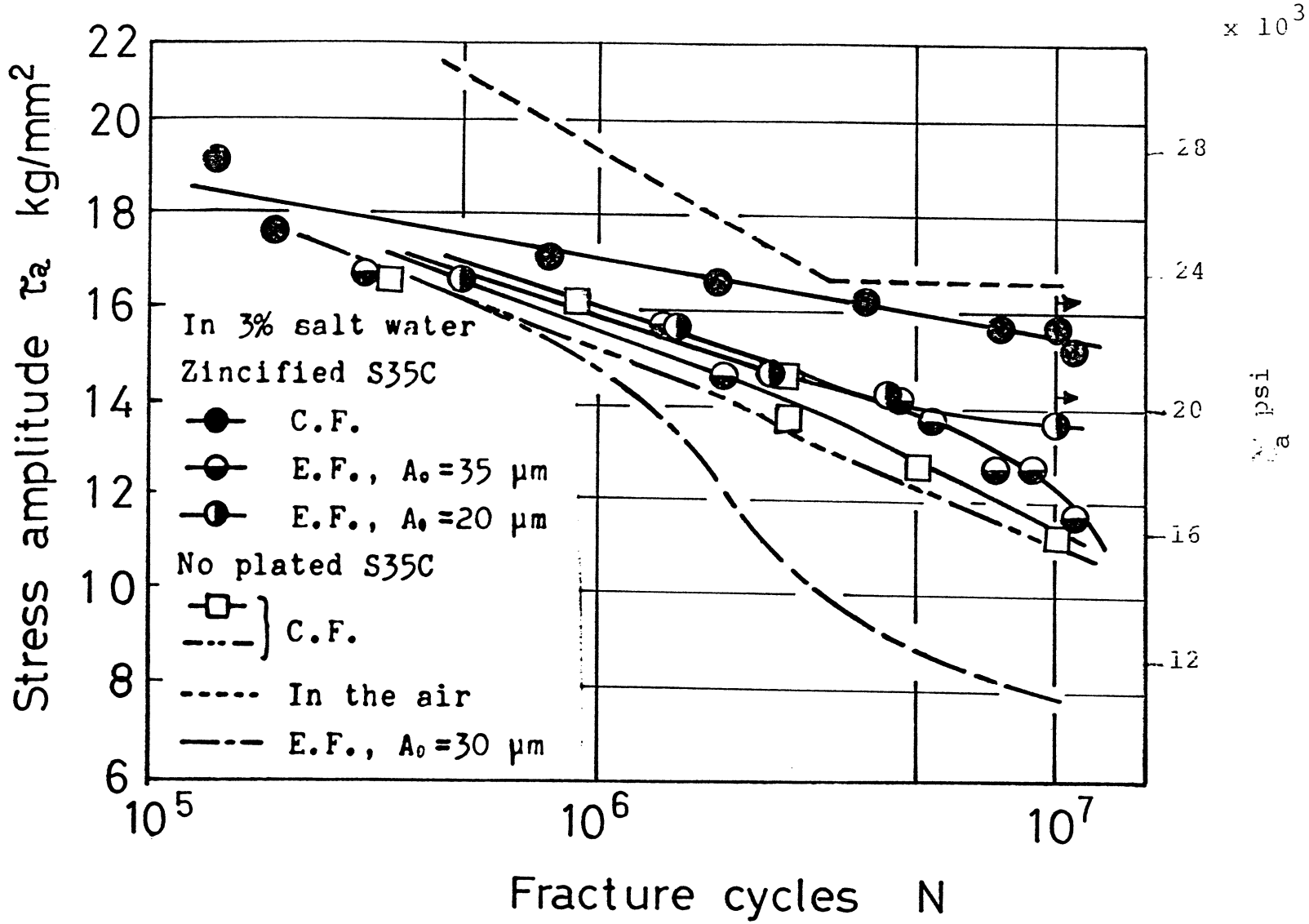


Fig.20 S-N curves of zincified S35C fatigue test pieces

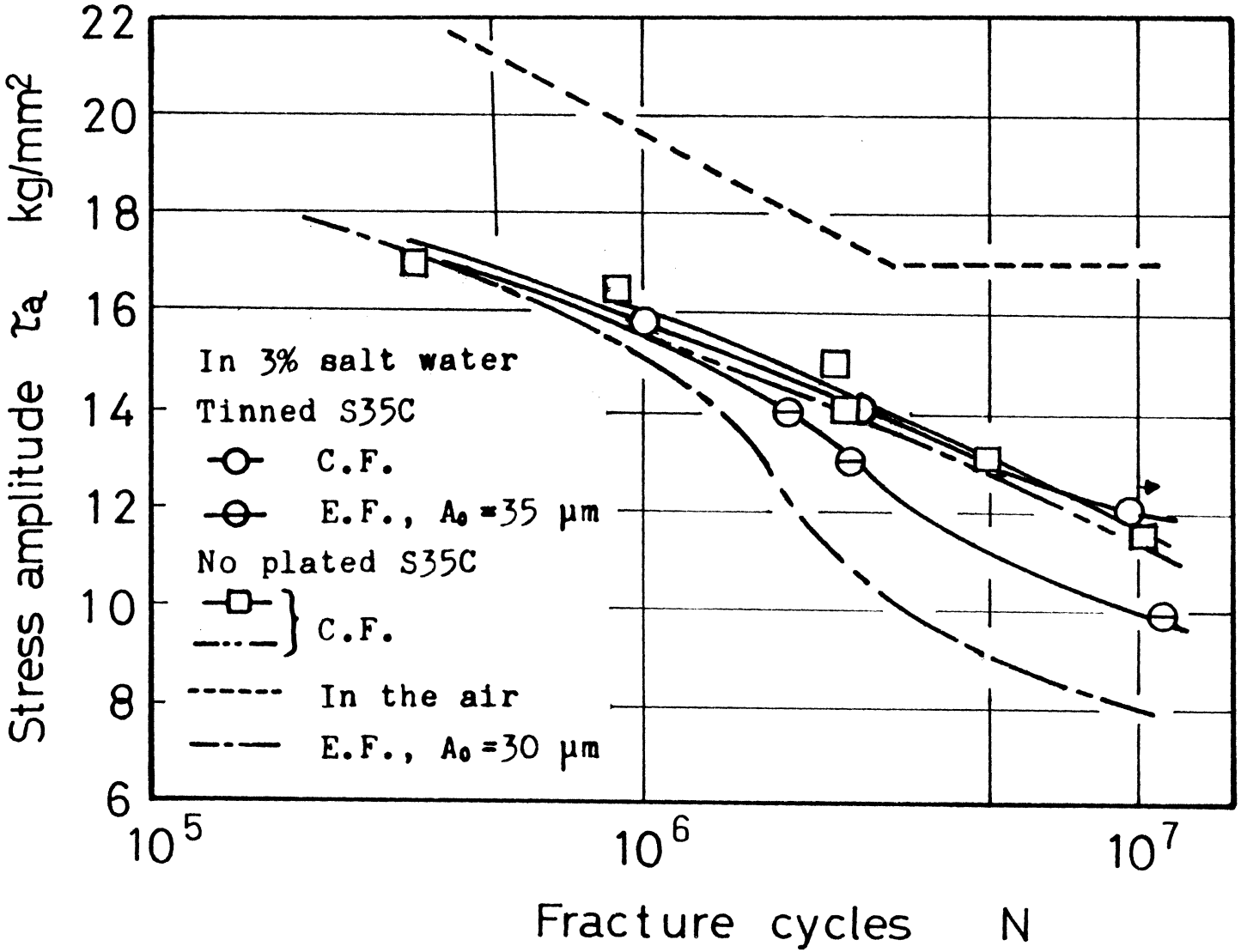


Fig.21 S-N curves of tinned S35C fatigue test pieces in 3% salt water (to be compared with the results of Fig.4)

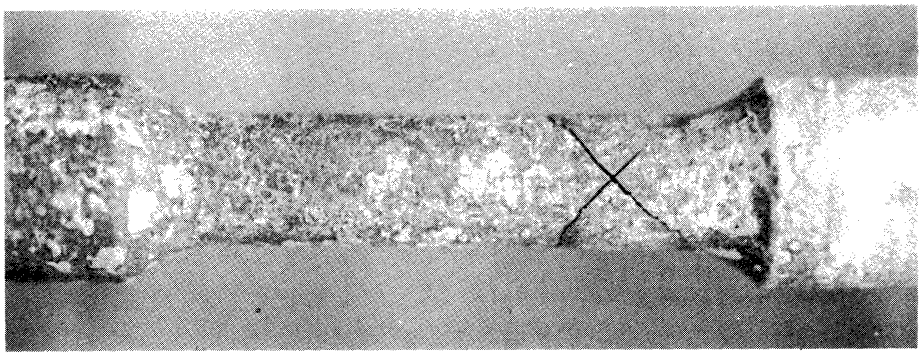

Zincified S35C test piece,
$\tau_a$=16.0 Kg/mm$^2$, N=7.64x10$^6$

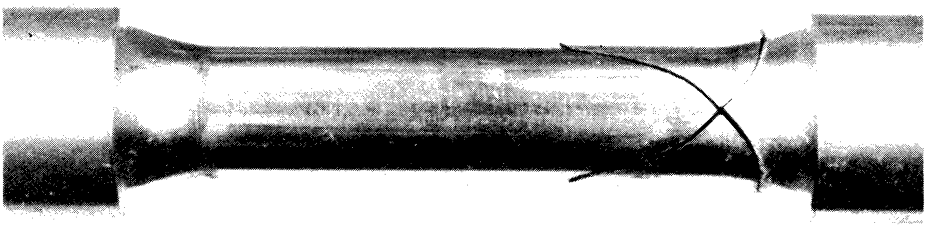

Tinned S35C test piece,
$\tau_a$=16.0 Kg/mm$^2$, N=1.10x10$^6$

Fig.22 Fracture in the corrosion fa e

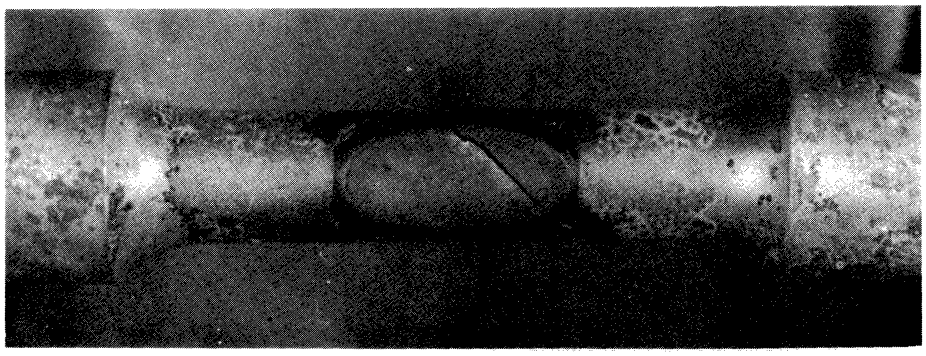

Zincified S35C test piece,
$\tau_a$=15.0 Kg/mm$^2$, h=0.5 mm,
N=1.95x10$^6$

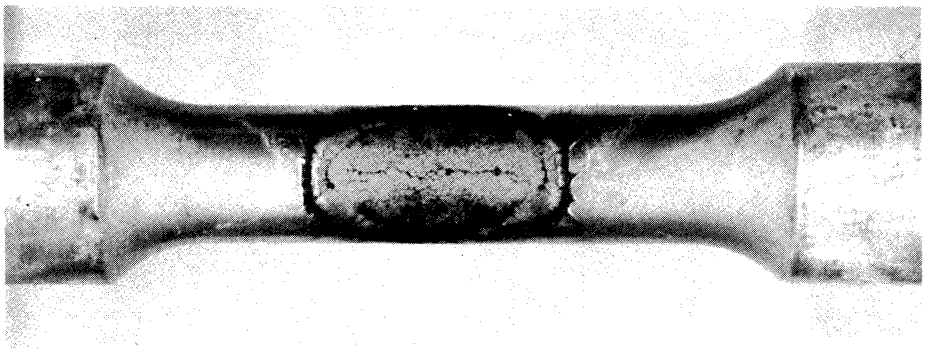

Tinned S35C test piece,
$\tau_a$=11.0 Kg/mm$^2$, h=0.5 mm,
N=6.84x10$^6$

Fig.23 Fracture in erosion fatigue

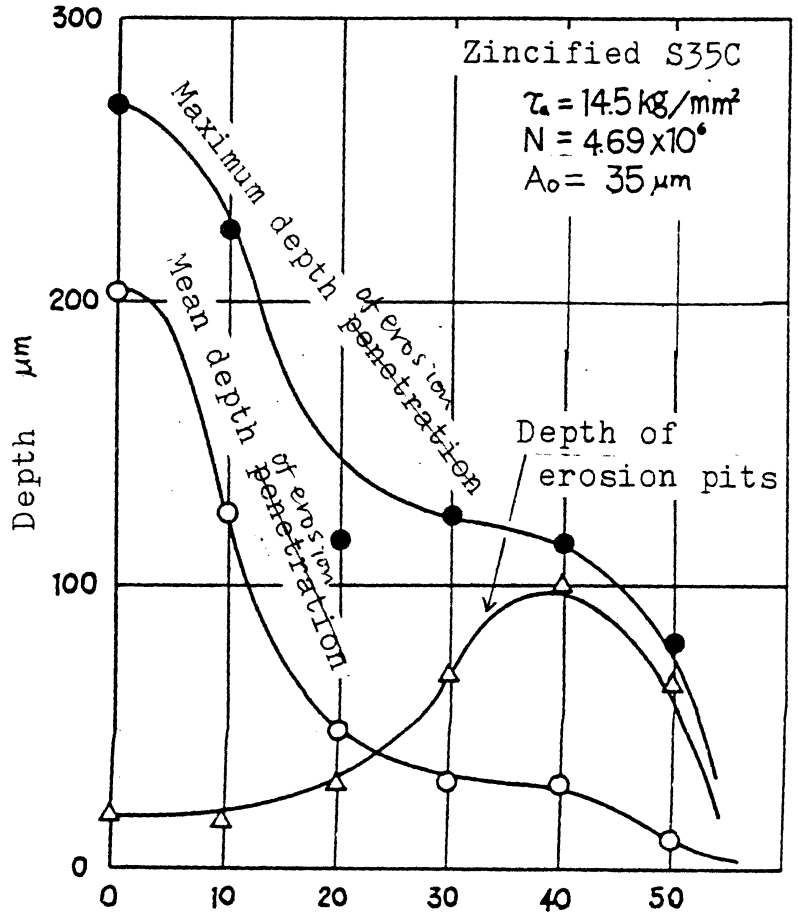


Fig.24 Maximum and mean distance from the virgin surface to the erosion surface and depth of the maximum pit itself on the zincified fatigue test pieces.

Maximum and mean distance from the virgin surface to the erosion surface and depth of the maximum pit itself on the zincified fatigue test pieces.